Metals **2015**, *5*, 777-789; doi:10.3390/met5020777

OPEN ACCESS

metals

ISSN 2075-4701

www.mdpi.com/journal/metals/

Article

Manufacturing Ultrafine-Grained Ti-6Al-4V Bulk Rod Using Multi-Pass Caliber-Rolling

Taekyung Lee [1], Donald S. Shih [2], Yongmoon Lee [3] and Chong Soo Lee [3,*]

[1] Department of Mechanical Engineering, Northwestern University, Evanston, IL 60208, USA; E-Mail: taekyung.lee@northwestern.edu

[2] Boeing Research & Technology, St. Louis, MO 63166, USA; E-Mail: donald.s.shih@boeing.com

[3] Graduate Institute of Ferrous Technology, Pohang University of Science and Technology (POSTECH), Pohang 790-784, Korea; E-Mail: ymlee0725@postech.ac.kr

* Author to whom correspondence should be addressed; E-Mail: cslee@postech.ac.kr; Tel.: +82-54-279-9001; Fax: +82-54-279-9099.

Academic Editor: Heinz Werner Höppel

Received: 11 March 2015 / Accepted: 30 April 2015 / Published: 15 May 2015

Abstract: Ultrafine-grained (UFG) Ti-6Al-4V alloy has attracted attention from the various industries due to its good mechanical properties. Although severe plastic deformation (SPD) processes can produce such a material, its dimension is generally limited to laboratory scale. The present work utilized the multi-pass caliber-rolling process to fabricate Ti-6Al-4V bulk rod with the equiaxed UFG microstructure. The manufactured alloy mainly consisted of alpha phase and showed the fiber texture with the basal planes parallel to the rolling direction. This rod was large enough to be used in the industry and exhibited comparable tensile properties at room temperature in comparison to SPD-processed Ti-6Al-4V alloys. The material also showed good formability at elevated temperature due to the occurrence of superplasticity. Internal-variable analysis was carried out to measure the contribution of deformation mechanisms at elevated temperatures in the manufactured alloy. This revealed the increasing contribution of phase/grain-boundary sliding at 1073 K, which explained the observed superplasticity.

Keywords: multi-pass caliber-rolling; grain refinement; internal-variable theory; Ti-6Al-4V

---

1. Introduction

Titanium and its alloys have attracted attention from various fields such as structural-material, biomedical, munitions, and information-technology industries. In particular, Ti-6Al-4V alloy has been a key material in aerospace industries since it was developed in 1954 [1]. The alloy possesses a superior strength-to-weight ratio that increases the fuel efficiency of rocket and aircraft. It also exhibits excellent corrosion resistance and mechanical stability at various temperatures. Finally, the alloy has good formability at elevated temperatures after applying a certain thermomechanical process due to the superplasticity [2–4].

Many researchers have focused on the fact that grain refinement can improve mechanical properties of titanium alloys. The increasing fraction of grain boundaries act as barriers against dislocation slip, leading to grain-boundary strengthening. In addition, the grain refinement provides the increasing sources of grain-boundary sliding and hence induces the superplastic behavior at elevated temperatures. It is thus natural that ultrafine-grained (UFG) titanium alloys have been actively studied for decades [5–9]. To attain the UFG structure, most of previous works have utilized a severe plastic deformation (SPD) process, such as equal-channel angular pressing (ECAP) and high-pressure torsion (HPT) [10]. However, the manufactured samples were generally 10s of centimeters in length, which were limited to laboratory scale.

To produce a UFG bulk rod applicable to the industries, the authors have introduced a multi-pass caliber-rolling process as an alternative to the conventional SPD processes. Caliber-rolling machine includes several calibers with various sizes and shapes (e.g., oval and circular) in its rolls by which a multi-axial deformation is imposed on a workpiece during the process. Since Kimura *et al.* [11] reported the considerable mechanical improvement in a caliber-rolled low-alloy steel, related studies have been actively carried out with various materials [12–19]. Nevertheless, studies on caliber-rolled titanium alloys have just begun in spite of its importance both in academia and industry [20–22]. A UFG bulk rod was successfully manufactured by caliber-rolling Ti-6Al-4V alloy in this work. The researchers investigated microstructures and tensile properties of the manufactured material and discussed mechanisms of grain refinement and superplasticity.

2. Materials and Methods

Ti-6Al-4V rod was machined with a diameter of 28 mm and a length of 150 mm. The head part was made to be conical to insert a material into a pair of calibers. The beta-transus temperature of this alloy was reported to be 1268 K [9]. The Ti-6Al-4V rod was solution-treated at 1323 K for 2 h followed by quenching in a water bath to induce a fine lath structure. This alloy was then soaked in a furnace at 1073 K for 1 h and caliber-rolled in the ambient atmosphere. The caliber-rolling process used in this work consists of six deformation passes. First, third, and fifth calibers are oval-shaped, while second, fourth, and sixth calibers are circular. The sample was inserted in a caliber, rotated by 90 degrees, and then immediately inserted in the next caliber for each deformation path, as illustrated in Figure 1. There was a single reheating process at 1073 K for 2 min after the fourth deformation pass. The sample was air-cooled after the sixth deformation pass. The total reduction of area was determined to be 85%.

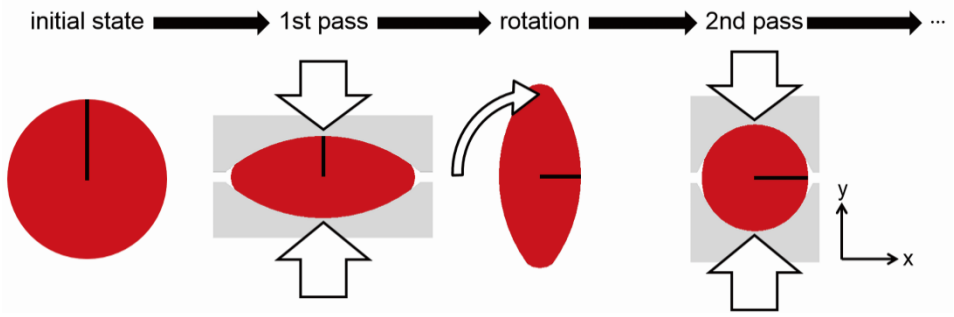

Figure 1. Schematic illustration of multi-pass caliber-rolling process.

Disc samples with a diameter of 3 mm were obtained from the caliber-rolled alloy, and then mechanically thinned with 240-grit SiC papers to a thickness less than 200 μm. Afterwards, they were jet-polished at 22 V and 265 K in a solution containing 40 mL of $HClO_4$, 240 mL of 2-butoxy ethanol, and 400 mL of methanol. Transmission electron microscope (TEM) was used to observe microstructures at 200 kV with JEM-2100F FE-TEM machine (JEOL, Tokyo, Japan). Grain size was measured from the image using the linear intercept method [23]. Meanwhile, other discs were mirror-polished with 1 μm alumina powder and 0.25 μm colloidal silica for electron backscatter diffraction (EBSD) analysis. The analysis was performed at 20 kV with Quanta 3D FEG machine (FEI, Hillsboro, OR, USA).

Tensile properties were measured using rod-type specimens whose gauge length and diameter were 6 and 3 mm, respectively. Instron 8862 machine (INSTRON, Norwood, MA, USA) was used for both room- and high-temperature tensile tests. Room-temperature tensile test was carried out at a strain rate of 5×10^{-3} s^{-1} with an extensometer to obtain reliable data. High-temperature tensile test was conducted in a halogen furnace at two temperature conditions (873 K and 1073 K) and two strain rates (5×10^{-3} s^{-1} and 5×10^{-4} s^{-1}). Each sample was heated for 10 min before commencing the test. Load-relaxation test (LRT) was conducted in a similar manner to the high-temperature tensile test, except that the samples were deformed up to a true strain of 0.2 and then hold to investigate the load relaxation behavior. The obtained LRT data were converted into stress-strain rate relationship based on the following equation [24]:

$$\sigma = P(L_0 + X - P/K)/A_0L_0 \quad (1a)$$

$$\dot{} = -(dP/dt)(L_o + X - P/K) \quad (1b)$$

$$K^{-1} \approx C_m + L_0/A_0E \quad (1c)$$

where P is load, L_o is the gauge length, A_o is the cross-sectional area of gauge region, X is the displacement, C_m is the elastic compliance of testing machine, and E is Young's modulus of Ti-6Al-4V alloy. Strain-rate-jump test (SRJT) was performed at 1073 K, during which a strain rate changed from 5×10^{-4} s^{-1} to 5×10^{-3} s^{-1} at a true strain of 0.6. Strain-rate sensitivity (m) was determined as follows:

$$m = \partial \log \sigma / \partial \log \dot{} \quad (2)$$

3. Results

Figure 2 demonstrates the manufactured caliber-rolled Ti-6Al-4V bulk rod. The length and diameter of the rod was approximately 1200 and 10 mm, respectively. It is also noted that the length can be even increased by tailoring the dimension of initial material. Such a large dimension enables the caliber-rolled rod to be directly used in the industry. Indeed, the authors fabricated a dental implant fixture with this material, which exhibited satisfying mechanical strength and fatigue resistance both in ambient atmosphere and simulated body fluid [21].

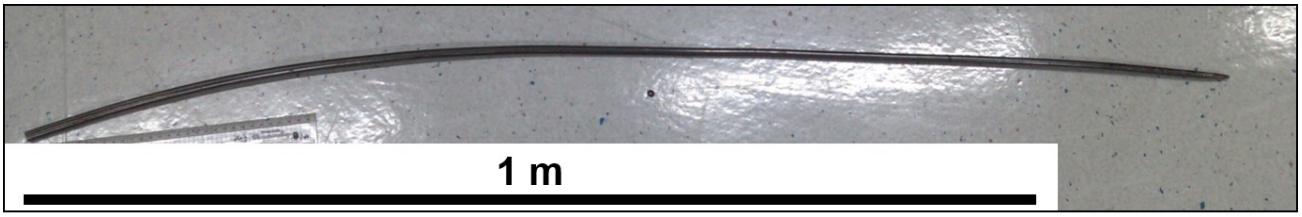

Figure 2. Ti-6Al-4V bulk rod manufactured by the multi-pass caliber-rolling process.

The grain structure of caliber-rolled rod was observed by TEM analysis as shown in Figure 3. It is obvious that the rod possessed the UFG structure with a grain size of 0.2 ± 0.05 μm. Such a strong grain refinement has thus far been accomplished by SPD processes. For example, Ko *et al.* [25] achieved a similar UFG structure with a mean grain size of ~0.3 μm after applying four-pass ECAP deformation at 873 K; however, the length of fabricated sample was much shorter (80 mm) compared to the present UFG rod.

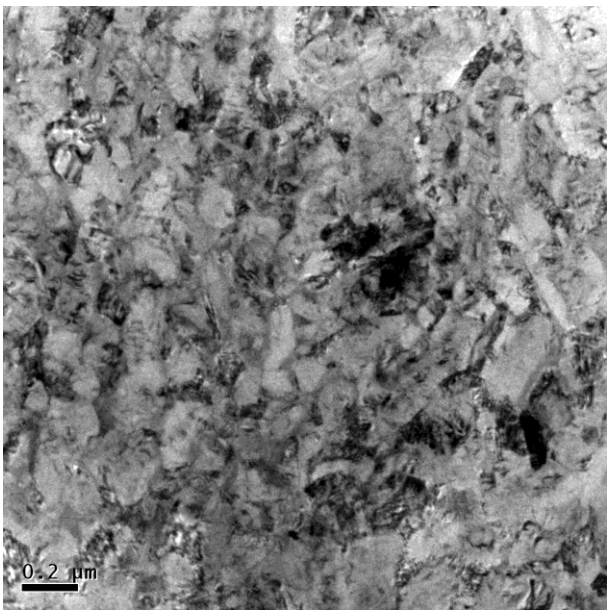

Figure 3. Transmission electron microscope (TEM) micrograph of caliber-rolled Ti-6Al-4V rod. The image was taken perpendicular to the rolling direction (RD).

Figure 4 presents the EBSD results for the investigated materials. The solution-treated microstructure consisted of martensitic laths as intended. Beta phase was not confirmed in this alloy, as reported in the literature [26,27]. Two types of martensitic laths were observed; coarse primary laths were formed first,

and then fine secondary laths were generated between the primary laths [28]. The latter occupies the most area in the solution-treated alloy, whose lath thickness is less than 5 μm. The similar lath structure with no presence of beta phase was confirmed after the heating step prior to the caliber-rolling (*i.e.*, 1073 K for 1 h), although the thickness was increased to ~10 μm. The beta fraction increased to 6% after the caliber-rolling. Figure 5 shows two types of beta constituents; most of them exist as a form of nano-sized beta precipitations, while fragmented beta lamellae are also observed. The beta lamellae were formed parallel to the RD and the thickness was measured to be ~0.2 μm or less. Chao *et al.* [27] attributed this type of phase transformation to adiabatic heating and strain-induced transformation. A fraction of high-angle grain boundaries of 0.6–0.8 was confirmed in Ti-6Al-4V alloys groove-rolled at 923–1023 K [22]. Similar results are expected in the present material as both rolling processes have the similar deformation mechanism.

The confidence index (CI) of caliber-rolled rod was too low to provide meaningful microstructural information. Tirumalasetty *et al*. [29] ascribed the low CI in UFG alloys to distorted Kikuchi patterns in region with high dislocation density. Alternatively, the EBSD analysis was conducted after annealing the caliber-rolled alloy at 873 K for 1 h, followed by water-quenching; such a condition was reported to minimize recrystallization and maintain the texture in this material [30]. Figure 4c,d demonstrate two types of grains: fine and coarse-grain groups. The fine grains are closer to the original microstructure of caliber-rolled alloy because the clear image and high CI of coarse grains imply the formation of microstructure during the subsequent annealing process. It should be noted that the fine grains are equiaxed in both planes, supporting the conclusion from TEM observation that the caliber-rolling gave rise to the equiaxed UFG structure for the present material.

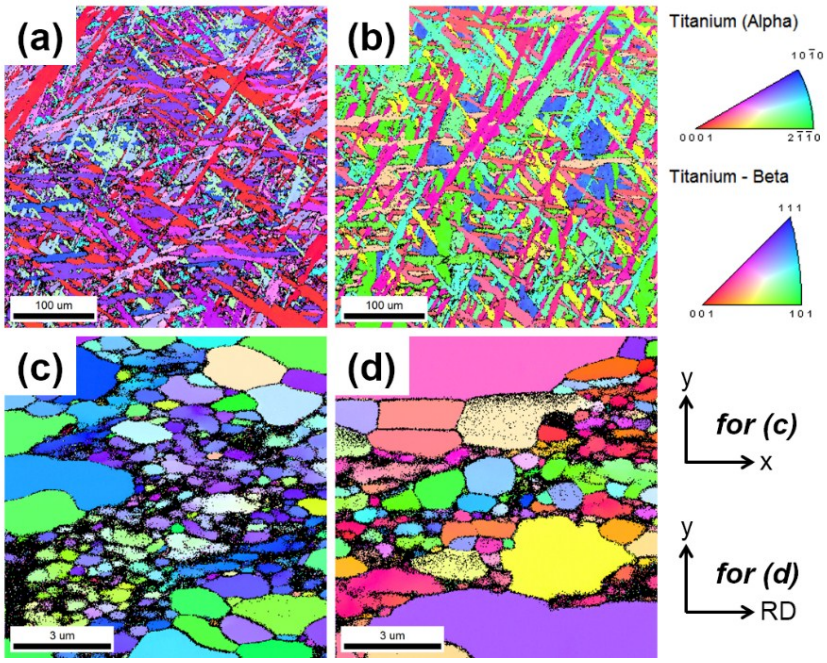

Figure 4. Electron backscatter diffraction (EBSD) pole figure map of the investigated Ti-6Al-4V rod: (**a**) solution-treated; (**b**) heat-treated prior to the caliber-rolling; and (**c**,**d**) caliber-rolled and annealed alloys. Figure 4c is a plane perpendicular to the RD, while Figure 4d is parallel to the RD. The black dots indicate the area of confidence index (CI) ≤ 0.1. The *x* and *y* axes are demonstrated in Figure 1.

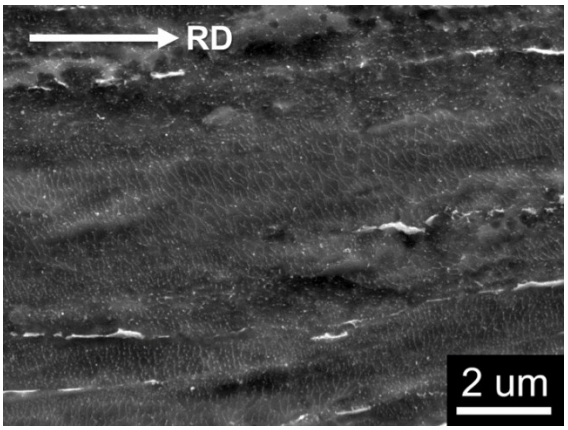

Figure 5. SEM micrograph of the caliber-rolled Ti-6Al-4V rod. The dark and bright areas indicate alpha and beta phases, respectively. The image was taken parallel to the RD marked as the arrow in the micrograph.

Figure 6 presents the texture of the caliber-rolled rod in the form of RD inverse pole figure. The alloy exhibited the fiber texture with the basal planes parallel to the RD. The fraction of beta phase is small enough to be neglected. Narayana Murty *et al.* [22] recently reported the similar texture in Ti-6Al-4V alloys groove-rolled at 873–1023 K, although their texture showed stronger orientation along <10-10> and <2-1-10> directions. According to the work [22], the relatively randomized texture observed in the present alloy may be attributed to higher deformation temperature related to martensite decomposition and phase transformation during the deformation process as well as the annealing treatment.

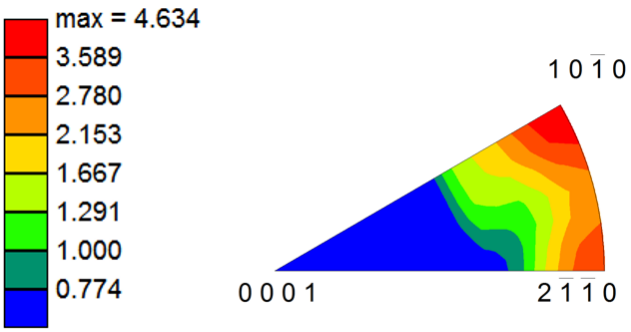

Figure 6. RD inverse pole figure for the caliber-rolled Ti-6Al-4V rod obtained by EBSD.

The manufactured UFG rod can be utilized in two ways in the industry. First, the material can be directly machined to be used for biomedical products, such as dental implant fixture, bone screw, bone plate, and micro-drill [1]. Room-temperature tensile properties are important in this case to ensure the resistance to fatigue fracture for biomedical uses. Second, the rod can be further processed at elevated temperature for automobile and aerospace industries, which requires the evaluation of high-temperature mechanical properties. Therefore, the tensile properties of the caliber-rolled Ti-6Al-4V alloy were investigated at both room and elevated temperatures.

Figure 7 shows room-temperature tensile properties of the caliber-rolled rod as well as UFG Ti-6Al-4V alloys in the literature [5–8]. The caliber-rolled rod provided the high yield stress (YS = 1345 MPa) and ultimate tensile stress (UTS = 1425 MPa) due to its UFG structure and resultant grain-boundary strengthening. The tensile properties of the manufactured alloy was compared with SPD-processed UFG

Ti-6Al-4V alloys in terms of the product of strength and elongation; such an approach has been widely used in the field of structural materials as strength increases in sacrifice of elongation in many cases [31]. The UFG bulk Ti-6Al-4V rod fabricated in this work exhibited the value of 18,525 MPa%, as shown in Figure 7b, which was comparable with most of UFG Ti-6Al-4V alloys in the literature.

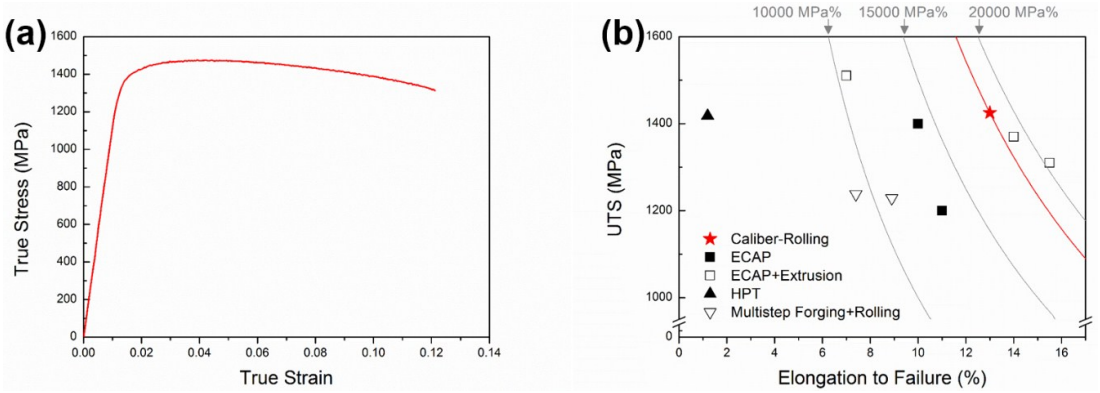

Figure 7. (**a**) True stress-strain curve of caliber-rolled Ti-6Al-4V rod at room temperature and (**b**) comparison of the tensile properties of various ultrafine-grained (UFG) Ti-6Al-4V alloys [5–8].

Figure 8a shows flow curves of the caliber-rolled alloy at elevated temperatures. Increasing deformation temperature or decreasing strain rate increased the ductility in sacrifice of strength. High-temperature deformation mechanisms at each condition were discussed in Section 4 on the basis of the internal-variable theory. It is of particular note that the caliber-rolled rod deformed at 1073 K and 5×10^{-4} s^{-1} exhibited the different characteristics than the others. The sample recorded a total elongation of 967% as shown in the inset of Figure 8a, whose flow curve showed a long plateau as generally found in superplastic materials. In addition, the SRJT results shown in Figure 8b provided a strain-rate sensitivity of 0.44 for the caliber-rolled Ti-6Al-4V at 1073 K. A material with a strain-rate sensitivity of 0.3–0.8 is considered to possess superplasticity [32]. All of these factors suggest the superplastic behavior of the present bulk rod at the high temperature, which will be useful in the related industries.

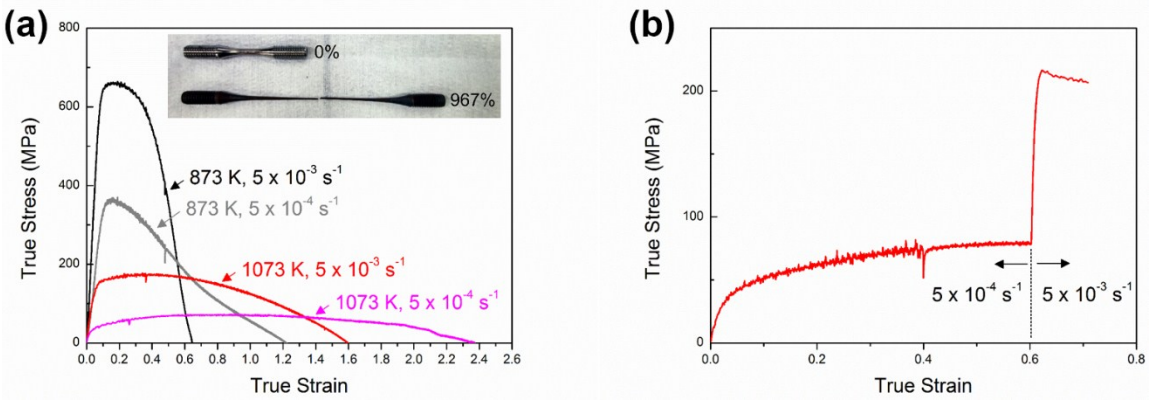

Figure 8. High-temperature tensile properties of caliber-rolled Ti-6Al-4V rod: (**a**) true stress-strain curve at elevated temperatures and (**b**) SRJT results obtained at 1073 K. The inset in Figure 8a compares the undeformed specimen and the sample deformed at 1073 K and 5×10^{-4} s^{-1}.

4. Discussion

The caliber-rolling process gave rise to the strong grain refinement by which the grain size became similar to those refined by the SPD processes. Such a microstructural evolution can be understood in terms of the dynamic globularization [33–36]. A groove formed at the phase/grain boundaries splits a platelet into several pieces by deepening along the boundary in the platelet. The broken-up lamellae are transformed into globular grains to stabilize the surface energy.

Two factors contributed to the effective dynamic globularization and resultant grain refinement in the caliber-rolled Ti-6Al-4V alloy. First, the present alloy consisted of fine martensitic laths prior to the caliber-rolling process. According to the literature [27,37,38], such a microstructure is beneficial for the grain refinement through dynamic globularization because an initial lamellar thickness directly affects a final grain size. Second, the globularizing fraction increases with increase in an applied strain following an Avrami-type equation in Ti-6Al-4V [39]. The authors have proven that the caliber-rolling imposes more than twice as high strain than a conventional rolling with the same reduction of area [30]. In this work, the equivalent strain was determined to be 0.7, 1.2, 1.9, 2.4, 3.3, and 4.0 after the one- to six-pass caliber-rolling in a two-phase titanium alloy. This is attributed to the redundant strain accumulating without the volume change of workpiece [40].

Superplastic behavior was confirmed in the manufactured alloy at 1073 K and 5×10^{-4} s^{-1}. The high-temperature deformation data were interpreted on the basis of internal-variable theory to investigate the deformation mechanisms. Ha and Chang [41] suggested this theory to measure the contribution of grain matrix deformation (GMD) and phase/grain-boundary sliding (P/GBS) to deformation behavior at elevated temperatures. In the internal-variable theory, stress is composed of internal stress of long-range dislocation interactions (σ^I) and friction stress of short-range dislocation-lattice interactions (σ^F). Strain rate consists of the rate of internal strain ($\acute{\imath}$), non-recoverable plastic strain ($\acute{\alpha}$), and P/GBS ($\acute{\eta}$) strain. Among these factors, the friction stress and internal strain rate are negligible under the present conditions, providing stress and strain rate as follows:

$$\sigma = \sigma^I + \sigma^F \approx \sigma^I \tag{3a}$$

$$\acute{\varepsilon} = \acute{\imath} + \acute{\alpha} + \acute{\eta} \approx \acute{\alpha} + \acute{\eta} \tag{3b}$$

The internal stress, non-recoverable plastic strain rate, and P/GBS strain rate at a deformation temperature of T are determined from the following relations:

$$(\sigma^*/\sigma^I) = \exp(\acute{\alpha}^*/\acute{\alpha})^p \tag{4a}$$

$$\acute{\alpha}^* = \nu^I (\sigma^*/G)^{n(I)} \exp(-Q^I/RT) \tag{4b}$$

$$(\acute{\eta}/\acute{\eta}_o) = [(\sigma - \Sigma_\eta)/\Sigma_\eta]^{1/M} \tag{4c}$$

$$\acute{\eta}_o = \nu^\eta(\Sigma_\eta/\mu^\eta)^{n(\eta)} \exp(-Q^\eta/RT) \tag{4d}$$

Here, σ^* and Σ_η are stress for GMD and P/GBS, respectively. $\acute{\alpha}^*$ and $\acute{\eta}_o$ are their conjugate reference strain rates. ν^I and ν^η are the jump frequency for dislocations. Q^I and Q^η are the activation energy for GMD and P/GBS, respectively. R is the gas constant and other parameters are material constants [4].

Figure 9 shows LRT results and corresponding internal-variable analysis. The GMD curve deviated from the experimental data at lower strain rates of Figure 9a and almost entire range of Figure 9b. These deviations were corrected by the P/GBS curve. It is thus concluded that P/GBS was not activated at 873 K and a strain rate of 5×10^{-3} s^{-1}, whereas both mechanisms contributed to the high-temperature deformation in the other cases. The relative contribution of each mechanism was quantified on the basis of the LRT data. At 873 K and a strain rate of 5×10^{-4} s^{-1}, GMD mainly contributed to the deformation behavior (92% for GMD and 8% for P/GBS). Similar results were obtained at 1073 K and a strain rate of 5×10^{-3} s^{-1} (85% for GMD and 15% for P/GBS) from the extrapolated data in Figure 9b. These results explain why the superplasticity was not observed under the three conditions mentioned above.

On the other hand, the contribution of P/GBS significantly increased at 1073 K and a strain rate of 5×10^{-4} s^{-1} (55% for GMD and 45% for P/GBS). This is rationalized in light of the decreasing activation energy for deformation with increasing temperature and decreasing strain rate. The authors have reported that the activation energy decreased to that for interphase/grain-boundary diffusion under such conditions, resulting in the increasing contribution of P/GBS [4]. This conclusion is also supported by the fact that the friction stress for P/GBS decreased as the deformation temperature increased; the value of $\log \Sigma_\eta$ was −2.7 at 873 K and −5.7 at 1073 K. This is in good accord with the superplastic behavior observed at 1073 K and 5×10^{-4} s^{-1}.

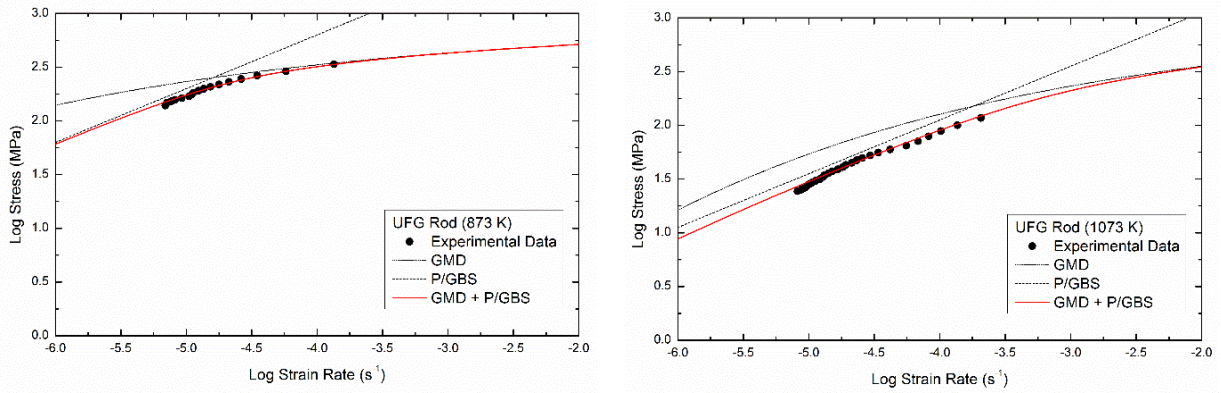

(**a**) (**b**)

Figure 9. Internal-variable analysis of caliber-rolled Ti-6Al-4V rod at (**a**) 873 K and (**b**) 1073 K.

5. Conclusions

In this work, the multi-pass caliber-rolling process successfully manufactured Ti-6Al-4V bulk rod with the UFG microstructure. The dimension of the manufactured rod (1200 mm in length) was significantly larger than most UFG Ti-6Al-4V samples fabricated by SPD processes and large enough to be directly used in the industry. The length can be even increased by tailoring the dimension of initial material. The alloy consisted of equiaxed ultrafine grains with a mean size of 0.2 μm. Such an effective grain refinement originated from the fine lath structure in the initial material and redundant strain accumulating without the volume change of workpiece. A small amount of beta particles was formed during the caliber-rolling process due to adiabatic heating and strain-induced phase transformation. The caliber-rolled rod showed the fiber texture with the basal planes parallel to the RD. The grain refinement through the caliber-rolling affected the grain-boundary strengthening at room temperature and superplastic

behavior at high temperature. The product of strength and elongation of the alloy at room temperature was calculated to be 18525 MPa%, which was similar to the values of most SPD-processed UFG Ti-6Al-4V alloys in the literature. The manufactured rod exhibited the superplastic behavior at 1073 K and 5×10^{-4} s^{-1}. The internal-variable analysis revealed the increasing P/GBS contribution to deformation under these conditions, while GMD controlled the deformation at the lower temperature and/or higher strain rate.

Acknowledgments

The authors gratefully acknowledge the financial support from The Boeing Company for the present research.

Author Contributions

T. Lee and C.S. Lee conceived and designed the experiments; T. Lee performed all experiments except for EBSD, analyzed the data, and wrote the paper; D.S. Shih and C.S. Lee guided the direction of the work and contributed reagents/materials/analysis tools; Y. Lee carried out the entire EBSD analyses; all authors participated in discussions.

Conflicts of Interest

The authors declare no conflict of interest.

References

1. Lee, Y.T. *Titanium*; Korea Metal Journal: Seoul, Korea, 2009.
2. Park, C.H.; Ko, Y.G.; Park, J.-W.; Lee, C.S. Enhanced superplasticity utilizing dynamic globularization of Ti-6Al-4V alloy. *Mater. Sci. Eng. A* **2008**, *496*, 150–158.
3. Semiatin, S.L.; Fagin, P.N.; Betten, J.F.; Zane, A.P.; Ghosh, A.K.; Sargent, G.A. Plastic flow and microstructure evolution during low-temperature superplasticity of ultrafine Ti-6Al-4V sheet material. *Metall. Mater. Trans. A* **2010**, *41*, 499–512.
4. Lee, T.; Kim, J.H.; Semiatin, S.L.; Lee, C.S. Internal-variable analysis of high-temperature deformation behavior of Ti-6Al-4V: A comparative study of the strain-rate-jump and load-relaxation tests. *Mater. Sci. Eng. A* **2013**, *562*, 180–189.
5. Mishra, R.S.; Stolyarov, V.V.; Echer, C.; Valiev, R.Z.; Mukherjee, A.K. Mechanical behavior and superplasticity of a severe plastic deformation processed nanocrystalline Ti-6Al-4V alloy. *Mater. Sci. Eng. A* **2001**, *298*, 44–50.
6. Salishchev, G.A.; Galeyev, R.M.; Valiakhmetov, O.R.; Safiullin, R.V.; Lutfullin, R.Y.; Senkov, O.N.; Froes, F.H.; Kaibyshev, O.A. Development of Ti-6Al-4V sheet with low temperature superplastic properties. *J. Mater. Process. Technol.* **2001**, *116*, 265–268.
7. Semenova, I.P.; Raab, G.I.; Saitova, L.R.; Valiev, R.Z. The effect of equal-channel angular pressing on the structure and mechanical behavior of Ti-6Al-4V alloy. *Mater. Sci. Eng. A* **2004**, *387–389*, 805–808.

8. Saitova, L.R.; Höppel, H.W.; Göken, M.; Semenova, I.P.; Valiev, R.Z. Cyclic deformation behavior and fatigue lives of ultrafine-grained Ti-6AL-4V ELI alloy for medical use. *Int. J. Fatigue* **2009**, *31*, 322–331.
9. Park, C.H.; Kim, J.H.; Yeom, J.-T.; Oh, C.-S.; Semiatin, S.L.; Lee, C.S. Formation of a submicrocrystalline structure in a two-phase titanium alloy without severe plastic deformation. *Scr. Mater.* **2013**, *68*, 996–999.
10. Azushima, A.; Kopp, R.; Korhonen, A.; Yang, D.Y.; Micari, F.; Lahoti, G.D.; Groche, P.; Yanagimoto, J.; Tsuji, N.; Rosochowski, A.; *et al*. Severe plastic deformation (SPD) processes for metals. *CIRP Ann. Manuf. Technol.* **2008**, *57*, 716–735.
11. Kimura, Y.; Inoue, T.; Yin, F.; Tsuzaki, K. Inverse temperature dependence of toughness in an ultrafine grain-structure steel. *Science* **2008**, *320*, 1057–1060.
12. Yin, F.; Hanamura, T.; Inoue, T.; Nagai, K. Fiber texture and substructural features in the caliber-rolled low-carbon steels. *Metall. Mater. Trans. A* **2004**, *35*, 665–677.
13. Torizuka, S.; Ohmori, A.; Narayana Murty, S.V.S.; Nagai, K. Effect of strain on the microstructure and mechanical properties of multi-pass warm caliber rolled low carbon steel. *Scr. Mater.* **2006**, *54*, 563–568.
14. Inoue, T.; Yin, F.; Kimura, Y. Strain distribution and microstructural evolution in multi-pass warm caliber rolling. *Mater. Sci. Eng. A* **2007**, *466*, 114–122.
15. Lee, T.; Park, C.H.; Lee, D.-L.; Lee, C.S. Enhancing tensile properties of ultrafine-grained medium-carbon steel utilizing fine carbides. *Mater. Sci. Eng. A* **2011**, *528*, 6558–6564.
16. Lee, T.; Koyama, M.; Tsuzaki, K.; Lee, Y.-H.; Lee, C.S. Tensile deformation behavior of Fe–Mn–C TWIP steel with ultrafine elongated grain structure. *Mater. Lett.* **2012**, *75*, 169–171.
17. Chun, Y.S.; Lee, J.; Bae, C.M.; Park, K.-T.; Lee, C.S. Caliber-rolled TWIP steel for high-strength wire rods with enhanced hydrogen-delayed fracture resistance. *Scr. Mater.* **2012**, *67*, 681–684.
18. Lee, T.; Park, C.H.; Lee, S.-Y.; Son, I.-H.; Lee, D.-L.; Lee, C.S. Mechanisms of tensile improvement in caliber-rolled high-carbon steel. *Met. Mater. Int.* **2012**, *18*, 391–396.
19. Doiphode, R.; Kulkarni, R.; Narayana Murty, S.V.S.; Prabhu, N.; Prasad Kashyap, B. Effect of severe caliber rolling on superplastic properties of Mg-3Al-1Zn (AZ31) alloy. *Mater. Sci. Forum* **2012**, *735*, 327–331.
20. Lee, T.; Heo, Y.-U.; Lee, C.S. Microstructure tailoring to enhance strength and ductility in Ti–13Nb–13Zr for biomedical applications. *Scr. Mater.* **2013**, *69*, 785–788.
21. Jung, H.S.; Lee, T.; Kwon, I.K.; Kim, H.S.; Hahn, S.K.; Lee, C.S. Surface modification of multi-pass caliber-rolled Ti alloy with dexamethasone-loaded graphene for dental applications. *ACS Appl. Mater. Interfaces* **2015**, *7*, 9598–9607.
22. Narayana Murty, S.V.S.; Nayan, N.; Kumar, P.; Narayanan, P.R.; Sharma, S.C.; George, K.M. Microstructure-texture-mechanical properties relationship in multi-pass warm rolled Ti-6Al-4V alloy. *Mater. Sci. Eng. A* **2014**, *589*, 174–181.
23. Dieter, G.E. *Mechanical Metallurgy*; Metric, S.I., Ed.; McGraw-Hill: London, UK, 1988.
24. Lee, D.; Hart, E. Stress relaxation and mechanical behavior of metals. *Metall. Mater. Trans. B* **1971**, *2*, 1245–1248.

25. Ko, Y.G.; Lee, C.S.; Shin, D.H.; Semiatin, S.L. Low-temperature superplasticity of ultra-fine-grained Ti-6Al-4V processed by equal-channel angular pressing. *Metall. Mater. Trans. A* **2006**, *37*, 381–391.
26. Matsumoto, H.; Bin, L.; Lee, S.-H.; Li, Y.; Ono, Y.; Chiba, A. Frequent occurrence of discontinuous dynamic recrystallization in Ti-6Al-4V Alloy with α′ martensite starting microstructure. *Metall. Mater. Trans. A* **2013**, *44*, 3245–3260.
27. Chao, Q.; Hodgson, P.D.; Beladi, H. Ultrafine grain formation in a Ti-6Al-4V alloy by thermomechanical processing of a martensitic microstructure. *Metall. Mater. Trans. A* **2014**, *45*, 2659–2671.
28. Williams, J.C.; Taggart, R.; Polonis, D.H. The morphology and substructure of Ti-Cu martensite. *Metall. Mater. Trans. B* **1970**, *1*, 2265–2270.
29. Tirumalasetty, G.K.; van Huis, M.A.; Kwakernaak, C.; Sietsma, J.; Sloof, W.G.; Zandbergen, H.W. Unravelling the structural and chemical features influencing deformation-induced martensitic transformations in steels. *Scr. Mater.* **2014**, *71*, 29–32.
30. Lee, C.S.; Lee, T.; Kim, J.H.; Park, C.H. Fabrication of ultrafine-grained Ti-6Al-4V bulk sheet/rod for related industries and their mechanical characteristics. In Proceedings of the 8th Pacific Rim International Conference on Advanced Materials and Processing (PRICM 8), Waikoloa, HI, USA, 4–9 August 2013.
31. Bouaziz, O.; Allain, S.; Scott, C.P.; Cugy, P.; Barbier, D. High manganese austenitic twinning induced plasticity steels: A review of the microstructure properties relationships. *Curr. Opin. Solid State Mater. Sci.* **2011**, *15*, 141–168.
32. Reed-Hill, R.E.; Cribb, W.R.; Monteiro, S.N. Concerning the analysis of tensile stress-strain data using log dσ/dεp *versus* log σ diagrams. *Metall. Mater. Trans. B* **1973**, *4*, 2665–2667.
33. Seshacharyulu, T.; Medeiros, S.C.; Morgan, J.T.; Malas, J.C.; Frazier, W.G.; Prasad, Y.V.R.K. Hot deformation and microstructural damage mechanisms in extra-low interstitial (ELI) grade Ti-6Al-4V. *Mater. Sci. Eng. A* **2000**, *279*, 289–299.
34. Stefansson, N.; Semiatin, S.L. Mechanisms of globularization of Ti-6Al-4V during static heat treatment. *Metall. Mater. Trans. A* **2003**, *34*, 691–698.
35. Zherebtsov, S.; Murzinova, M.; Salishchev, G.; Semiatin, S.L. Spheroidization of the lamellar microstructure in Ti-6Al-4V alloy during warm deformation and annealing. *Acta Mater.* **2011**, *59*, 4138–4150.
36. Park, C.H.; Won, J.W.; Park, J.-W.; Semiatin, S.L.; Lee, C.S. Mechanisms and kinetics of static spheroidization of hot-worked Ti-6Al-2Sn-4Zr-2Mo-0.1Si with a lamellar microstructure. *Metall. Mater. Trans. A* **2012**, *43*, 977–985.
37. Park, C.H.; Park, J.-W.; Yeom, J.-T.; Chun, Y.S.; Lee, C.S. Enhanced mechanical compatibility of submicrocrystalline Ti-13Nb-13Zr alloy. *Mater. Sci. Eng. A* **2010**, *527*, 4914–4919.
38. Matsumoto, H.; Yoshida, K.; Lee, S.-H.; Ono, Y.; Chiba, A. Ti-6Al-4V alloy with an ultrafine-grained microstructure exhibiting low-temperature-high-strain-rate superplasticity. *Mater. Lett.* **2013**, *98*, 209–212.
39. Song, H.-W.; Zhang, S.-H.; Cheng, M. Dynamic globularization kinetics during hot working of a two phase titanium alloy with a colony alpha microstructure. *J. Alloys Compd.* **2009**, *480*, 922–927.

40. Maccagno, T.M.; Jonas, J.J.; Hodgson, P.D. Spreadsheet modelling of grain size evolution during rod rolling. *ISIJ Int.* **1996**, *36*, 720–728.
41. Ha, T.K.; Chang, Y.W. An internal variable theory of structural superplasticity. *Acta Mater.* **1998**, *46*, 2741–2749.